Preprint Title	A novel anatase TiO_2@MIL-101(Cr) nanocomposite for photocatalytic degradation of Bisphenol A
Authors	Yuan Tang, Xiaohong Yin, Manman Mu, Yue Jiang, Xiaoli Li, Hao Zhang and Tianwei Ouyang
Publication Date	08 Nov 2019
Article Type	Full Research Paper
Supporting Information File 1	supporting information (2).doc; 39.0 MB
ORCID® iDs	Xiaohong Yin - https://orcid.org/0000-0003-0976-6718

A novel anatase TiO_2@MIL-101(Cr) nanocomposite for photocatalytic degradation of Bisphenol A

Yuan Tang [a, b], Xiaohong Yin [a, b,*], Manman Mu [a, b,*], Yue Jiang [a, b], Xiaoli Li [a, b], Hao Zhang [a, b], Tianwei Ouyang [a, b]

[a] School of Chemistry and Chemical Engineering, Tianjin University of Technology, Tianjin 300384, PR China

[b] Tianjin Key Laboratory of Organic Solar Cells and Photochemical Conversion, Tianjin 300384, PR China

Corresponding author: Xiaohong Yin, yinxiaohong@tjut.edu.cn

Manman Mu, mumanman@tju.edu.cn

Abstract

A series of novel anatase TiO_2@MIL-101(Cr) composite was synthesized by solvothermal method for photocatalytic degrading bisphenol A (BPA). Compared with pure TiO_2 and MIL-101(Cr), these composites exhibited superior catalytic performance for the BPA photocatalytic degradation. The characterization results determined the chemical structure and combination between TiO_2 and MIL-101(Cr). The optical properties of the composites demonstrated enhanced catalytic efficiency with effectively separating the electron-hole pair and narrowing band gap. Moreover, the TiO_2 amount and surface area in the composites jointly influenced the activity of photocatalytic degradation of BPA, which, meanwhile, was evaluated by changing the initial pH, catalyst dosage and initial BPA concentration. Under optimal condition, 59% TiO_2@MIL-101(Cr) could reach 99.4% BPA degradation and the corresponding rate constant was 0.0138 min^{-1} in 240 min under UV irradiation. Furthermore, TiO_2@MIL-101(Cr) possessed the excellent stability and was reusable. The reasonable pathway of BPA degradation was proposed based on the detected intermediates during the degradation, where the oxidative radicals $\cdot O_2^-$ played a dominant role.

Keywords: Anatase TiO_2; TiO_2@MIL-101(Cr); Photocatalytic degradation of BPA; Synergistic effect; Photocatalytic mechanism

1. Introduction

Bisphenol A (BPA) is one of significant chemicals which has been widely used in epoxy resin and polycarbonate plastic [1]. Moreover, as a representative of endocrine disrupting chemicals (EDCs)，the excessive emission of BPA leads to endocrine disorder and environmental pollution which seriously threaten human health [2]. Nowadays, several techniques have been developed to removal of BPA from wastewaters, including physical absorption [3,4], biodegradation [5,6], chemical processes [7] and photocatalysis [8-13]. In view of low cost, less environmental pollution and high efficiency, photocatalysis has been regarded as a promising approach for removal of BPA.

As one of the most commonly used semiconducting photocatalyst, TiO_2 has attracted special attention for photocatalytic degradation of BPA by its safety, non-toxicity, stability and low cost [14]. However, the photocatalytic efficiency of TiO_2 is restricted because of its wide band gap (3.2 eV) and rapid recombination of photogenerated electron-hole pair. Yoshihisa et al. reported that the BPA solution was completely degraded to carbon dioxide by TiO_2 for 20 hours under the UV irradiation [15]. Moreover, pure TiO_2 is liable to be aggregated which result in reducing catalytic efficiency due to poor adsorption capacity and low surface area. Therefore, several methods were developed to raise the photocatalytic degradation activity of TiO_2, such as ion co-doping [16,17], noble metals or non-metal doping [18,19] and combining with other semiconductors [20, 21].

Metal-organic frameworks (MOFs) is an emerging porous crystal material, which is employed in catalysis, gas storage, drug delivery and separation [22-24]. Among numerous MOF materials, MIL-101(Cr) (Cr-MIL) attracts great interests due to large surface area, high stability and easy for functionalization. However, the catalytic performance of Cr-MIL is limited because of the deficient active sites. Thus, a promising strategy to enhance the photocatalytic performance is the incorporation with TiO_2 [25-29]. To date, some studies about Cr-MIL-based photocatalysts in the photocatalytic production of H_2 [30], degradations of RhB [31] and hydrogen sulfide [32] have been reported. Gong et al. reported a novel g-C_3N_4/MIL-101(Fe) heterostructure for BPA degradation were exhibited in the presence of persulfate. Zhang et al. reported a Fe_3O_4@beta-CD/rGO heterostructure with excellent catalytic performances for photocatalytic hydrogen production [33,34]. However, there are few studies on TiO_2@MIL-101(Cr) for the

photocatalytic degradation of BPA without additional activator.

Herein, a series of TiO_2@MIL-101(Cr) composites named as TMCr were fabricated *via* two-step synthetic procedure. The physical-chemical properties of the composites were characterized by X-ray diffraction (XRD), Scanning electron microscopy (SEM), Brunner - Emmet - Teller (BET) measurements, UV-vis diffuse reflectance spectra, Transmission electron microscopy (TEM), X-ray photoelectron spectroscopy (XPS) and Photoluminescence spectroscopy (PL). The composites were used for photocatalytic degradation of aqueous BPA under UV light. The influence of the TiO_2 amount, initial pH value, catalyst dosage and initial BPA concentration were investigated. Moreover, the stability and the reusability of the composite were also evaluated. Finally, the degradation intermediates were detected by high performance liquid chromatography-mass spectrometry for supporting the proposition of degradation pathway of BPA.

2. Experimental

2.1. Materials

Chromic nitrate ($Cr(NO_3)_3 \cdot 9H_2O$) was purchased from Shanghai Aladdin Biochemical Technology. Terephthalic acid (H_2BDC) and sodium hydroxide (NaOH) were obtained from Tianjin Guangfu Fine Chemical. Hydrofluoric acid (HF), bisphenol A (BPA) and titanium tetrachloride ($TiCl_4$) were purchased from Tianjin Fuchen Chemical. Anhydrous ethanol, N, N-dimethylformamide (DMF), tetrahydrofuran (THF), benzoquinone (BQ), potassium iodide (KI) and isopropanol were purchased from Tianjin Damao Chemical. Methanol and acetonitrile were purchased from Concord Chemical, chromatographic grade. All of the chemical reagents were of analytic purity and used directly without further purification.

2.2. Synthesis of Cr-MIL and TiO_2

Cr-MIL was synthesized according to the reported studies [35]. TiO_2 was prepared by $TiCl_4(THF)_2$ as a precursor. Specifically, 1 mL of $TiCl_4$ was added to 10 mL of THF solution to form yellow $TiCl_4(THF)_2$ [36]. The obtained yellow solution and 20 mL DMF was transferred into a 75 mL Teflon-lined autoclave and heated at 220℃for 24 h. After cooled into room temperature,

the crude product was obtained by centrifugation, and washed with deionized water and ethanol for several times. The yielded white powder was dried overnight at 60 ℃.

2.3. Synthesis of TMCr

A series of X% TMCr composites are synthesized by two steps (X% refer to the mass content of TiO_2). Firstly, Cr-MIL was synthesized by the above solvothermal method. Secondly, 2 mL of $TiCl_4(THF)_2$, 0.1 g of Cr-MIL and 20 mL of DMF were respectively mixed in a Teflon-lined autoclave (75 mL) and heated at 220℃ for 24 h. The products obtained by centrifugation were washed several times with deionized water and ethanol for several times. Finally, the products were dried overnight at 60℃ to obtain 59% TMCr. A series of X% TMCr with different contents of TiO_2 (40, 70 and 85 wt%) were prepared by similar method with different additions of $TiCl_4(THF)_2$ (1 mL, 3 mL and 4 mL). In addition, a new self-assembled Cr-MIL, called Cr-MIL-1, was synthesized by adding 0 ml $TiCl_4$ into the mixed solution in a similar way.

2.4. Characterization

XRD was performed using a Rigaku Corporation diffractometer operated by Cu Kα irradiation source at 40 kV and 40 mA. SEM images (ZEISS-Merlin) were used to investigate the morphologies of the catalysts. The structure of the samples was revealed by HRTEM and TEM. EDS equipped with TEM is used for element mapping analysis of regions of interest. Nitrogen adsorption-desorption measurements were formed on an AUTOSORB-1C analyser. FT-IR of the catalysts were carried out under the Bruker Tensor-27 spectrometer, and KBr was used as a standard to detect the molecular structure of the catalysts. The surface element of chemical composition of the catalysts was investigated by XPS (Thermo Scientific ESCALAB250Xi). Using $BaSO_4$ as the reflection standard, the UV-vis diffuse reflectance spectra (DRS) were measured on Shimadzu UV-2550. Mott–Schottky analysis were carried out on a Chenhua CHI660E electrochemical workstation. The mineralization level of BPA was detected by a Total organic carbon (TOC) analyzer (TOC-L CPH, Shimaddan).

2.5. Adsorption performance of BPA

In order to explored adsorption performances of the as-prepared catalysts, 80 mL BPA

aqueous solution (50 mg/L) with 40 mg catalysts was stirred in dark for 90 minutes, 1.5 mL was taken out from the solutions periodically at a certain time interval using a syringe and filtered with syringe filters (PES, 0.45 μm). The concentrations of BPA were analyzed by high-performance liquid chromatograph (HPLC) equipped with C-18 column (Kromasil, C18, 5μm, 250×4.6 mm).

the adsorption capacity of BPA on the adsorbent is calculated as:

$$Q_t = V(C_0 - C_t)/m$$

Among them, C_0 is the initial BPA concentration, V is the BPA solution volume, C_t is the BPA concentration at a given time (t), and m is the adsorbent mass.

2.6. Photocatalytic activity of degrading BPA

In order to evaluate the photocatalytic degradation performance of the catalysts, 50 mg/L of BPA aqueous solution was degraded under ultraviolet light irradiation, and a 125 W mercury lamp was used as an ultraviolet light source. photocatalytic degradation experiment was carried out using 80 mL of BPA aqueous solution containing 40 mg of photocatalyst. It is noteworthy that sorption equilibrium was achieved by stirring suspension in a dark box for 90 min. After the light was turned on, 1.5 mL was sampled out from the solutions periodically at a certain time interval using a syringe and filtered with syringe filters. HPLC was used to detect the concentration of BPA.

3. Results and discussion

3.1. Characterization of photocatalysts

A series of X% TMCr composites was prepared by two-step synthetic procedure and the corresponding process is described in Fig.1. Firstly, Cr-MIL was synthesized using $Cr(NO_3)_3 \cdot 9H_2O$ and HF as raw materials. Subsequently, a predetermined mass ratio of $TiCl_4(THF)_2$ and Cr-MIL was mixed to obtain the X% TMCr materials by solvothermal process.

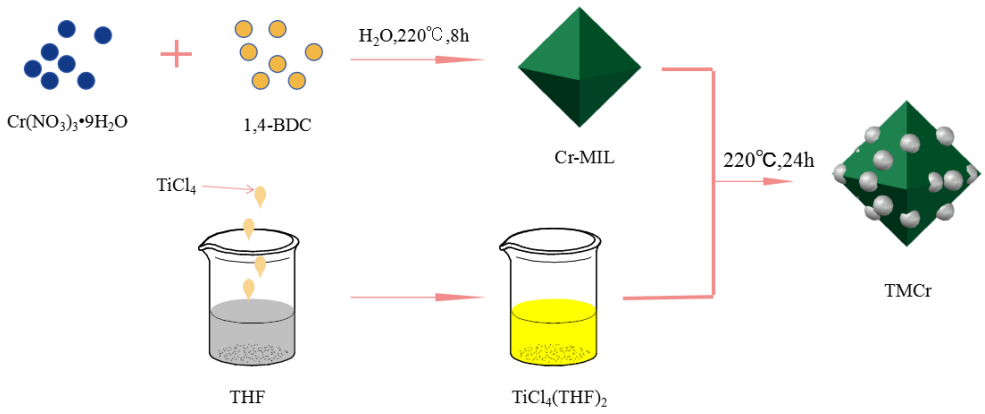

Fig.1. Schematic illustration of the synthesis of X% TMCr composite

The X-ray diffraction patterns of TiO_2 and X% TMCr composites are presented in Fig. 2. For the pure TiO_2, the typical peaks at 25.3°, 37.9°, 48.4°, 55.3°, 62.7°, 68.9° can be indexed to the anatase TiO_2 (JCPDS NO.01-0562) corresponding to the (101), (112), (200) and (005) plane, respectively. Moreover, it can be seen from Fig S1 that the diffraction peaks of Cr-MIL were consistent with the calculated one, demonstrating the successful preparation of Cr-MIL. Interestingly, the above characteristic peaks can be observed in X% TMCr composite, indicating that the MOF structure is still retained with the addition of TiO_2. In addition, the diffraction peak intensity of TMCr is significantly weakened compared to pure Cr-MIL. This illustrated that the crystallinity of composite decreased and the crystal structure became more disorderly than that of Cr-MIL. We speculated that the synthetic procedure of composite was similar to that of Cr-MIL, resulting in the further self-assembly process of Cr-MIL. Next, the SEM testing was conducted to verify the above thought.

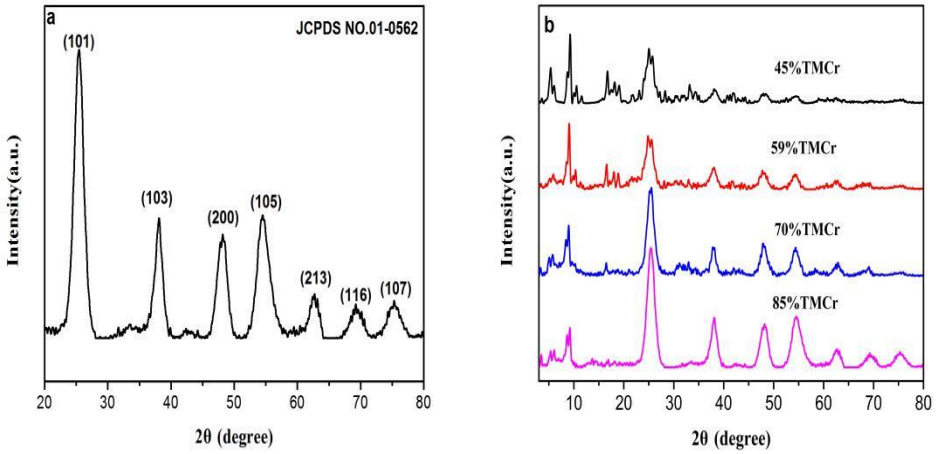

Fig.2. XRD patterns of (a)TiO_2, (b) X% TMCr

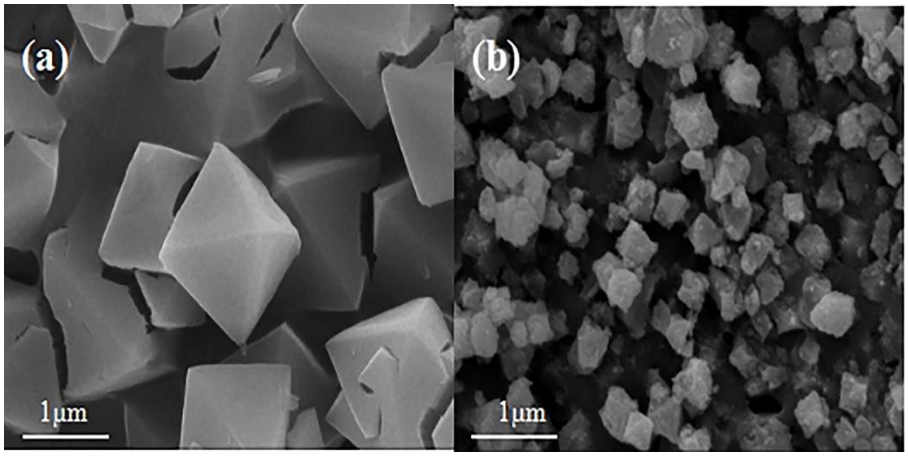

Fig.3. SEM images of (a) Cr-MIL, and (b) 59% TMCr

The morphologies of the Cr-MIL and X% TMCr were investigated by SEM. The as-prepared Cr-MIL presents regular octahedral shape and the particle size ranges from 800 nm to 1μm (Fig. 3a). It could be observed from Fig. S3(d) that the Cr-MIL-1 without the addition of TiO_2 still maintained octahedral shape but the particle size was smaller compared to Cr-MIL. The reason was that the synthesis temperature of the composite is close to that of Cr-MIL, caused by recombination of Cr-MIL. The SEM images of X% TMCr demonstrates the similar shape as the Cr-MIL and the particle size is about 300-500 nm, and the surface of composite is much rougher after the introduction of TiO_2 (Fig. S3). The structure of Cr-MIL in the composite is still retained with the addition of TiO_2, which is consistent with the results of XRD.

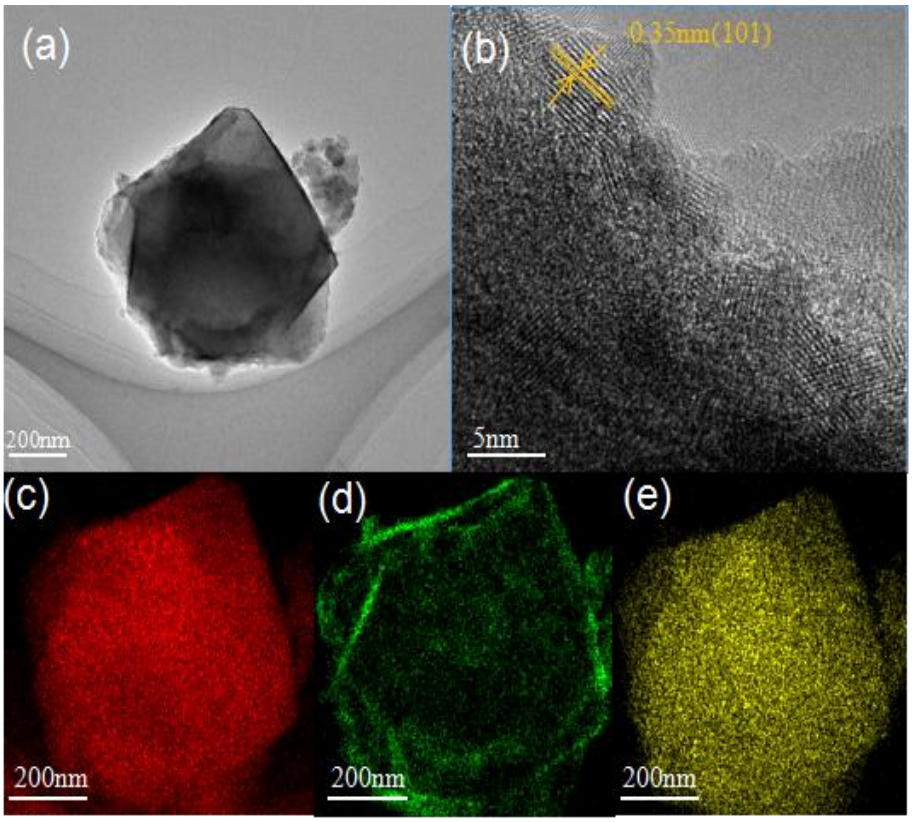

Fig.4. (a)TEM of 59% TMCr, (b) HRTEM of 59% TMCr, EDS mapping of 59% TMCr: (c) C, (d) Ti, (e) O.

To get further information about the microstructure of TMCr composite, TEM and HRTEM analysis was performed. As shown in Fig. 4a, the TiO_2 nanoparticles were tightly wrapped around the surface of Cr-MIL, indicating that TiO_2 nanoparticles have been firmly loaded on the surface of Cr-MIL *via* a solvothermal method. Additionally, the introduction of TiO_2 has no significant impact on the morphology of Cr-MIL. The corresponding HRTEM image in Fig 4b presents the lattice fringe with lattice spacing of 0.35 nm, corresponding to the (101) plane of the anatase TiO_2. The result is in accordance with the XRD and SEM analyses that TiO_2 has been successfully combined with Cr-MIL to form this composite. In addition, EDS characterization provide extra evidence of C, O, Ti and Cr elements in the TMCr composite (Fig. S4). The EDS elemental mapping indicates the uniform distribution of C, O, Ti elements in the TMCr composite.

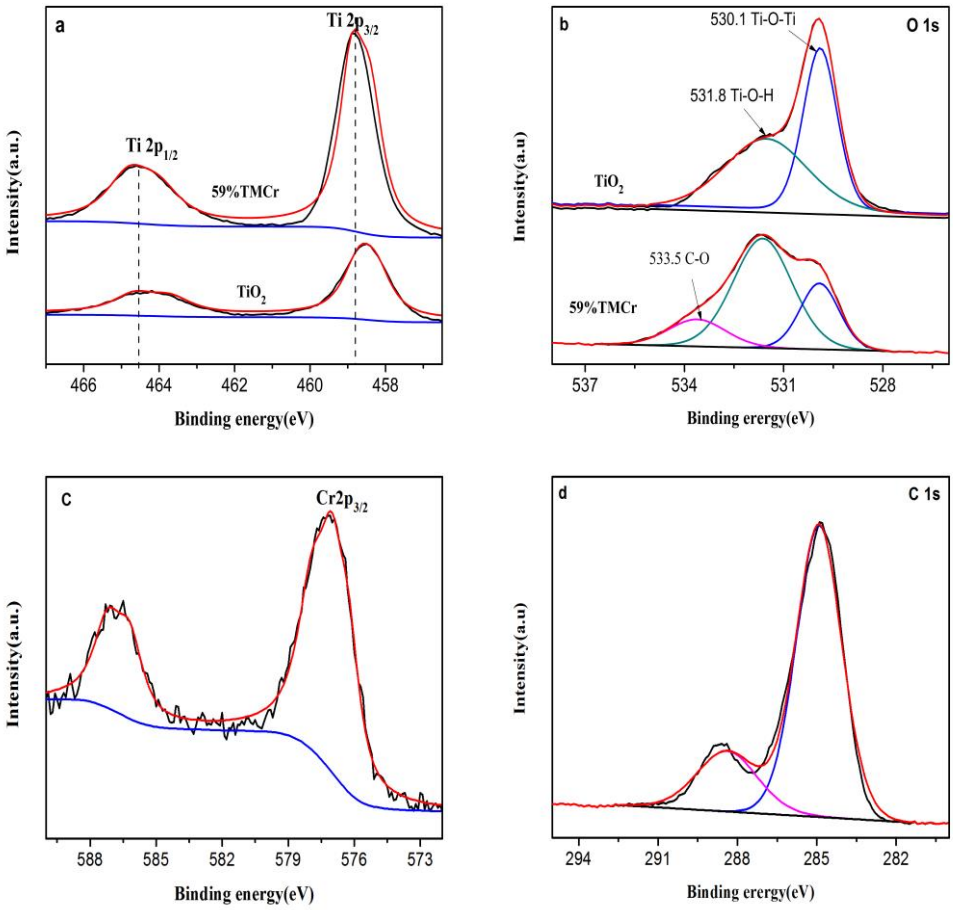

Fig.5. XPS patterns of TiO_2 and 59% TMCr: (a) Ti 2p, (b) O 1s, XPS patterns of 59% TMCr: (c) Cr 2p, (d) C 1s

The chemical composition of TMCr was further investigated by XPS. The XPS survey spectrum of 59%TMCr presented in Fig. S5 verified the presence of Ti, Cr, O and C element. The Ti 2p spectra of TiO_2 and this composite was shown in Fig. 5a and the characteristics binding energy at 458.5 and 464.3eV corresponded to the Ti $2p_{3/2}$ and Ti $2p_{1/2}$ energy levels indicated the existence of Ti^{4+} in a tetragonal structure [37]. Furthermore, this composite exhibited the larger Ti $2p_{3/2}$ and Ti $2p_{1/2}$ intensities, indicating that there was close interaction between Cr-MIL and TiO_2 [38]. Compared with TiO_2, the corresponding binding energies of this composite increased, revealing the presence of chemical bonding between Cr-MIL and TiO_2. The O1s spectra (Fig. 5(b)) show that the binding energies of O1s at 530.2 eV (Ti-O-Ti) and 531.8 eV appear which are caused by the lattice oxygen and Ti-O-H bonds of TiO_2. The relative content of Ti–O–Ti bond decreased but Ti–O–H content increased in 59% TMCr, indicating that the Ti-O bond of TiO_2 was

affected by Cr-MIL, in which the chemical environment has changed [40]. Notably, the peak at 533.5 eV is attributed to the C–O bond which implies the formation of heterostructures [40]. Moreover, it was observed from Fig 5c that two peaks at 586.8 eV and 577.2 eV corresponded the Cr $2p_{1/2}$ and Cr $2p_{3/2}$ signals, demonstrating the presence of Cr^{3+} [39]. 59% TMCr in C1s XPS spectra exhibited mainly two peaks at 284.8 and 288.7 eV, belonging to the C–C and O–C=O bond respectively (Fig. 5d).

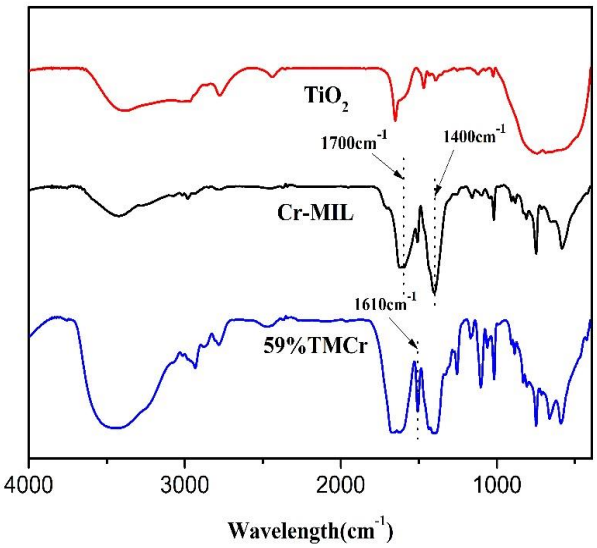

Fig.6. FT-IR patterns of Cr-MIL, TiO_2 and 59% TMCr.

Fig. 6 shows the FT-IR spectroscopy of Cr-MIL, TiO_2 and 59% TMCr. The peaks at 1700 cm^{-1}, 1400 cm^{-1} and 1610 cm^{-1} could be attributed to the aromatic C=O, O-C-O and C=C stretching vibration modes in the H_2BDC ligand [39]. A characteristic peaks pair of 800 cm^{-1} to 500 cm^{-1} is a typical absorption peak of TiO_2 [37]. In the case of TMCr composites, both the characteristic peaks assigned to the TiO_2 and Cr-MIL can demonstrate the coexistence of TiO_2 and Cr-MIL in the composites.

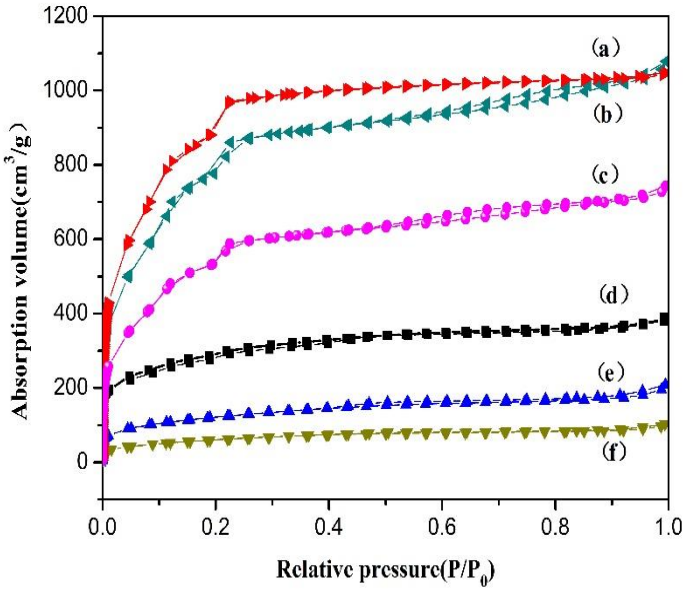

Fig.7. N_2 adsorption–desorption isotherms of materials, (a) Cr-MIL, (b) 42% TMCr, (c) 59% TMCr, (d) 70% TMCr, (e) 85% TMCr, (f) TiO_2.

Table 1 BET specific surface area of TiO_2, Cr-MIL and TMCr nanocomposites.

Sample	BET specific surface area ($m^2 \cdot g^{-1}$)
85% TMCr	416.12
70% TMCr	858.55
59% TMCr	2046.97
42% TMCr	3018.47
Cr-MIL	3293.44

Fig. 7 shows the N_2 adsorption-desorption isotherms of TiO_2, Cr-MIL and X% TMCr. The pure Cr-MIL exhibited type I isotherm according to the IUPAC classification, revealing that Cr-MIL is mainly microporous structure. Moreover, all the TMCr nanocomposites displayed type IV isotherms with a slight hysteresis loop. This is related to capillary condensation in a small number of mesopores, revealing the existence of mesopore. The corresponding BET specific surface areas are listed in Table 1. Obviously, with the increase of TiO_2 contents from 0 to 85 wt%, the BET specific surface area of X% TMCr reduced significantly from 3293.44 $m^2 \cdot g^{-1}$ to 416.12

$m^2 \cdot g^{-1}$. As is well known, the larger specific surface area of a photocatalyst is benefit for the carrier transport and adsorption of organic molecules, probably enhancing photocatalytic degradation performance of BPA solution. Besides, the TiO_2 content in X% TMCr should be considered as another critical factor to adjust photocatalytic degradation activity. Although the higher TiO_2 content contribute to improve photocatalytic degradation efficiency, the lower surface area of the composite might restrain the degradation efficiency. Therefore, the composite with the proper TiO_2 content and surface area should be considered.

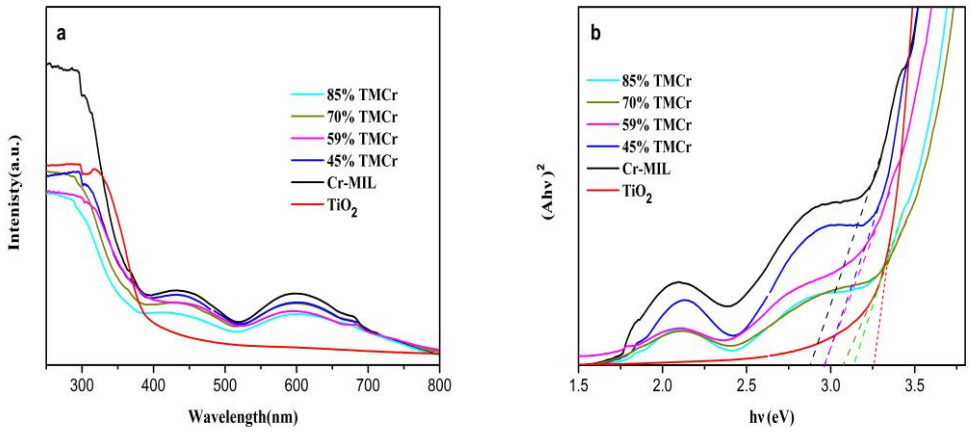

Fig.8. (a) UV-vis spectra of Cr-MIL, TiO_2 and X% TMCr photocatalysts, (b) plots of $(Ahv)^2$ as a function of vs. photon energy of Cr-MIL, TiO_2 and X% TMCr.

UV-Vis spectra of TiO_2, Cr-MIL and X% TMCr were examined to evaluate the optical properties of the samples, and the results were shown in Fig. 8. The pure TiO_2 owns an absorption edge around 380 nm. For Cr-MIL, besides the absorption edge near 360 nm, other absorption band in the region of 450-700 nm can be detected, which can be attributed to the d-d transition band of Cr^{3+} ions [40]. Based on the Kubelka-Munk function, the band gap of all the samples were estimated from the intercepts of the tangents of $(Ahυ)^2$ versus photon energy in Fig. 8b. Obviously, the band gap value of Cr-MIL and TiO_2 were calculated to be approximately 2.8 eV and 3.25 eV, respectively. In addition, the band gap value of TiO_2, Cr-MIL and X% TMCr nanocomposites were shown in Table 2, with the increase of TiO_2 contents, the band gap value gradually increased.

Table 2 The band gap value of TiO_2, Cr-MIL and X% TMCr nanocomposites.

Sample	the band gap(eV)
TiO_2	3.25
85% TMCr	3.15
70% TMCr	3.12
59% TMCr	2.95
42% TMCr	2.92
Cr-MIL	2.80

The photoelectron-hole recombination rate of TMCr was confirmed by PL emission spectrum. The PL spectrum of Cr-MIL showed a strong emission peak at around 418 nm (Fig.9). Obviously, the PL emission peak intensity of this composite diminished significantly when TiO_2 was introduced into the Cr-MIL framework, indicating a low recombination rate in TMCr as a result of the surface junction between TiO_2 and Cr-MIL for the effective separation of electron-hole pairs. The separation efficiency and lifetime of the carrier was respectively enhanced and extended by introducing TiO_2, which improved the photocatalytic degradation efficiency of this composite consequently.

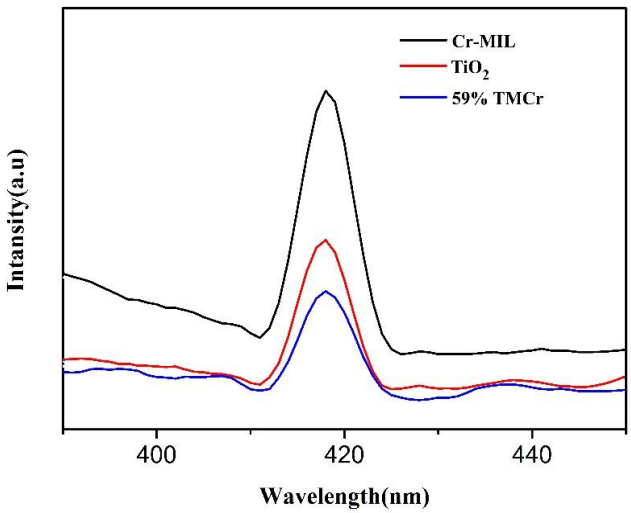

Fig.9. PL emission spectra of TiO_2, Cr-MIL and 59% TMCr

3.2. Adsorption performance

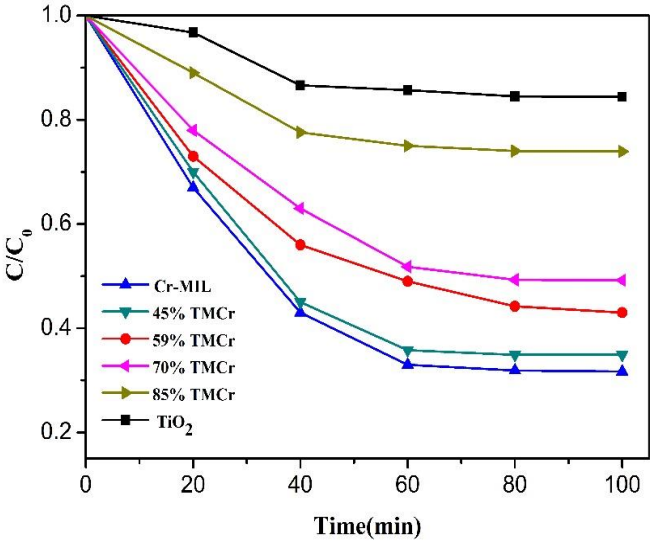

Fig.10. BPA adsorption curves of TiO_2, Cr-MIL and X% TMCr

The adsorption curves shown in Fig.10 present that pure Cr-MIL has the highest adsorption capacity on account of the maximum specific surface area (3293.44 $m^2 \cdot g^{-1}$) and the adsorption capacity of TMCr decreases with the increase of TiO_2 amount which is related to the specific surface area of TMCr. Table 3 shows the equilibrium capacities of Cr-MIL, TiO_2 and X% TMCr. Cr-MIL samples have a large BPA adsorption with a corresponding adsorption property of 69.0 $mg \cdot g^{-1}$. With the increase of the loading of TiO_2 from 45% to 85%, the adsorption properties of the composite are 65.1 $mg \cdot g^{-1}$, 57.0 $mg \cdot g^{-1}$, 50.8 $mg \cdot g^{-1}$, 26.1 $mg \cdot g^{-1}$, respectively. Adsorption properties of the TMCr was improved with the increase of specific surface area, but the introduction of TiO_2 leading to an enhanced photocatalytic degradation performance. So, we explored the collaborative influence of the Cr-MIL adsorption and the TiO_2 incorporation to achieve optimal degradation efficiency.

Table 3 The adsorption capacity of TiO_2, Cr-MIL and X% TMCr nanocomposites.

Sample	Q_t ($mg \cdot g^{-1}$)
TiO_2	15.6
85% TMCr	26.1
70% TMCr	50.8
59% TMCr	57.0
42% TMCr	65.1
Cr-MIL	69.0

3.3. Photocatalytic degradation activity

The photocatalytic degradation performance of TiO_2, Cr-MIL and 59% TMCr was evaluated by the degradation of BPA (50 mg/L) under UV irradiation, as shown in Fig.11. Obviously, the poor photocatalytic degradation efficiency (19%) was obtained in the absence of photocatalyst. Meanwhile, TiO_2 displayed moderate photocatalytic degradation performance for BPA degradation (29%). Whereas, no further degradation was conducted by the pure Cr-MIL under UV irradiation since a plenty of BPA absorbed in the catalyst was preferentially degraded but the degradation ability of Cr-MIL was relatively weak, leading a less change in BPA concentration of the system. More significantly, although TMCr composite had much less adsorption properties than Cr-MIL, after 30 minutes of UV irradiation, the BPA concentration dropped sharply and this composite showed the superior photocatalytic degradation efficiency with a degradation rate of BPA solution about 92% after 240 min. The reason was that the incorporation of TiO_2 increased the separation rate of electron-hole pairs, enhancing the degradation efficiency, which was in line with the PL results. Moreover, the TOC measurement indicated that BPA could be mineralized by this composite into CO_2 and H_2O with a degradation efficiency of 80% about 240 min. It was noteworthy that the TiO_2+Cr-MIL physical mixture had similar adsorption capacity to the composite but its degradation efficiency was obviously lower. This demonstrated that compare to the TiO_2+Cr-MIL mixture, the heterojunction of TMCr was benefit for the electron transfer between TiO_2 and Cr-MIL, resulting in the enhancement of photocatalytic degradation efficiency.

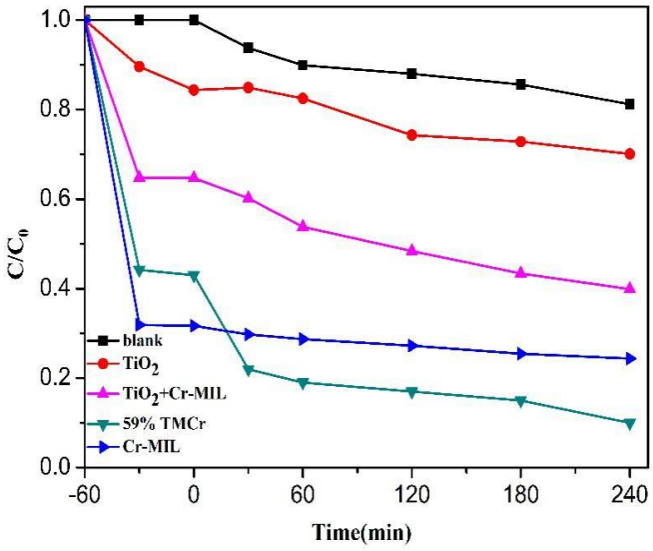

Fig.11. BPA photocatalytic degradation activity of different samples

Next, the photocatalytic degradation performances of the X% TMCr composites with different TiO_2 contents were further studied. As displayed in Fig. 12 (a), the adsorption capacities became weakened with the increase of TiO_2 content from 42% to 59% but the degradation efficiency were enhanced. We could discover from Table 1 that the BET specific surface area of 59% TMCr was 2046.97 m^2/g. Although it was lower than that of 42% TMCr, instead of its surface area, the content of TiO_2 was considered as the main factor to influence the degradation efficiency of BPA. Therefore, 59% TMCr exhibited the superior photo-degradation activity of BPA compare to 42% TMCr. However, both the adsorption and degradation performance were reduced when the TiO_2 content continued to be increased. As shown in Table 1, the specific surface area of X% TMCr sharply decreased from 858.45 m^2/g to 416.12 m^2/g with the increase of TiO_2 content from 70% to 85%, which was the main influence factor of BPA photo-degradation activity. It is noteworthy that the photocatalytic degradation activity of TMCr without any addition of TiO_2 was tested to prove the effect of particle size on photocatalytic degradation (Fig. S7). Compared with pure Cr-MIL, Cr-MIL-1 has similar adsorption capacity (74% for Cr-MIL-1 and 69% for Cr-MIL). However, the degradation rate constant (k) does not change significantly. In summary, the results show that the change of particle size has no obvious effect on photocatalytic degradation activity, and 59% TMCr possessed the superior surface area and appropriate TiO_2

content, so the excellent photo-degradation activity of BPA was gained.

As is well-known, the pH parameter is a significant factor to affect the surface charge properties of the photocatalyst. As shown in Fig. 12 (b), the influence of the initial pH on the BPA photocatalytic degradation was studied and the pH range was from 3 to 11, the photo-degradation efficiency reached its maximum of ~97% at pH 3 and it decreased gradually as pH increased. The corresponding kinetic constant also decreased from 0.0048 min^{-1} to 0.0034 min^{-1}(Fig. S8(b)). It has better degradation efficiency at pH = 3, which may be caused by the amphoteric behavior of the semiconductor material and the change in the surface charge properties of the TiO_2 photocatalyst. Therefore, pH = 3 was selected as the optimum condition for the study of the acid-base condition.

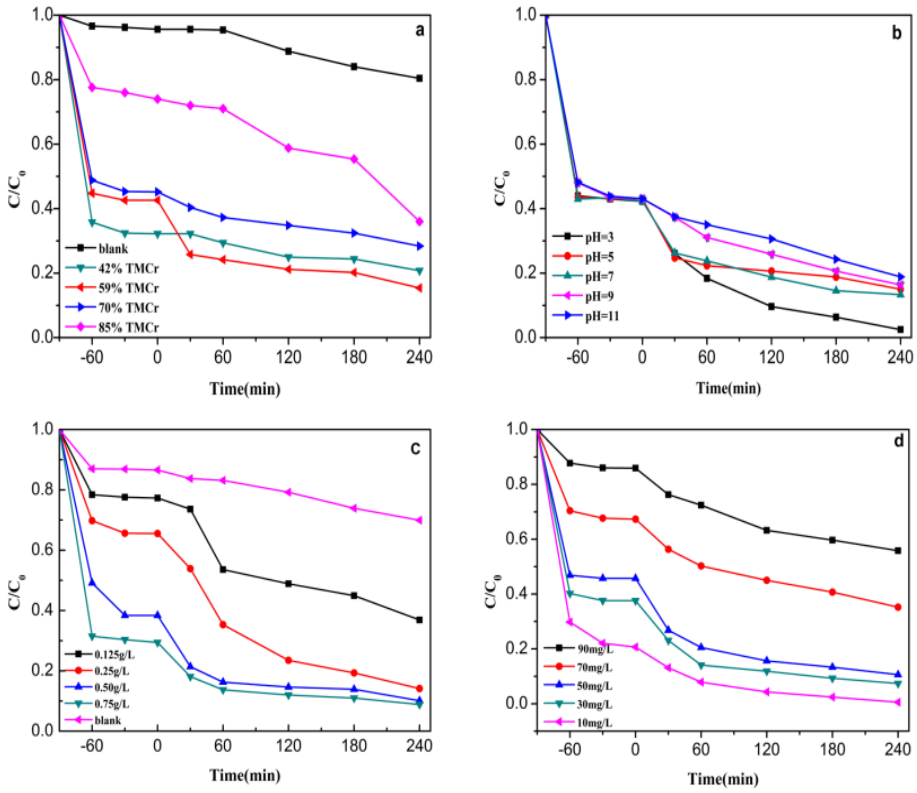

Fig.12. BPA degradation efficiency with TMCr in various reaction conditions: (a) different TiO_2: Cr-MIL weight ratios, (b) initial pH, (c) catalyst dosage, (d) initial BPA concentration.

As displayed in Fig. 12(c), the photocatalytic degradation efficiency was increased from 0.003 to 0.006 min^{-1} (Fig. S8(c)) with the increase of photocatalyst dosage from 0.125 to 0.75 g/L, whereas a negligible improvement of the degradation efficiency was investigated by further

increasing the catalyst dosage. This may be due to the excessive addition of catalysts, which caused aggregation of catalysts and shield the absorption of light. Therefore, 0.5g/L was chosen as the optimum catalyst dosage.

The effect of the initial BPA concentrations (10, 30, 50, 70, 90 mg/L) on the photocatalytic degradation of BPA was studied in Fig. 12(d). BPA could be removed 99.4% with the initial BPA concentration was 10 mg/L. And the degradation efficiency slightly dropped to 95.2% and 92.5% with initial BPA concentration increased up to 30 and 50 mg/L, respectively. It clearly shown that the degradation efficiency was reduced at the higher initial concentrations. This might be due to a large number of BPA adsorbed at a higher BPA concentration, resulting that adsorption of BPA reached saturation onto the catalyst surface and slow down photocatalytic degradation. The degradation efficiency of different BPA concentrations (10, 30, 50, 70 and 90 mg/L) is 0.0138, 0.0061, 0.0053, 0.0024, 0.0017 min^{-1}, respectively (Fig. S8(d)). The amounts of catalytic sites in low concentration of BPA solution is much larger than that of BPA, so the reaction was conducted. Nevertheless, the photocatalytic degradation efficiency decreased in higher concentration of BPA solution, indicating that the amount of generated catalytic sites was not enough for degrading BPA, so the reaction was limited. Thus, 10 mg/L was selected as the optimal initial concentration.

3.4. Recycle experiments of the TMCr for BPA photocatalytic degradation

Two important characteristics of photocatalysts involved in the reutilization are stability and recyclability. In this work, four cycles of BPA photocatalytic degradation were conducted by 59% TMCr under ultraviolet light. As shown in Fig. 13, no significant loss of photocatalytic degradation activity was observed after four photocatalytic degradation cycles, confirming the excellent stability and recyclability of 59% TMCr. In addition, it could be observed from Fig. S2 that the XRD characteristic peaks of used 59% TMCr had no significant change compare to the fresh one, further demonstrating that 59% TMCr exhibited the excellent stability.

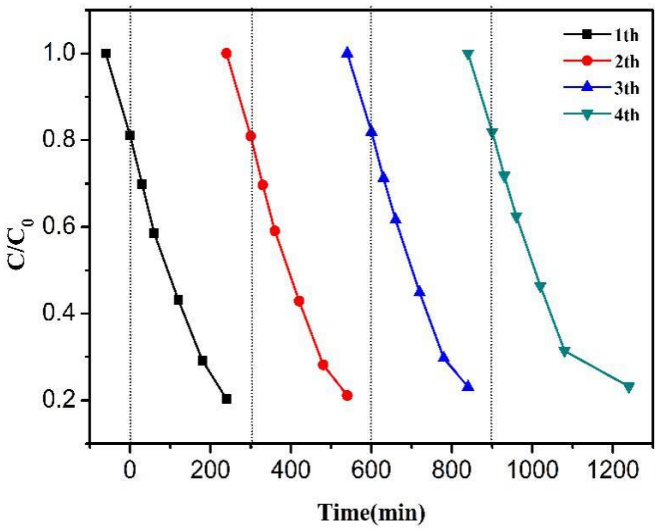

Fig.13. Recycle experiments of 59% TMCr for BPA degradation

3.5. Reactive species trapping experiments

In order to reveal the photocatalytic degradation mechanism of BPA using 59% TMCr composites, it is essential to investigate the reactive species in the photocatalytic degradation system. Free radical quenching agents such as isopropanol, KI and benzoquinone were used to quench the ·OH, h^+ and $\cdot O_2^-$, respectively [41]. As shown in Fig.14, the blank experiment without any free radical quenching agents, the photodegradation rate was 0.0084min^{-1}, and KI has no effect in reducing the photocatalytic degradation performance of 59% TMCr. And the BPA degradation efficiency declined from 0.0084 to 0.0067 min^{-1} with the addition of isopropanol. Once benzoquinone was added into the system, the degradation efficiency declined dramatically and the degradation rate decreased to 0.0012 min^{-1}, suggesting that $\cdot O_2^-$ is the major reactive species in this photocatalytic degradation system.

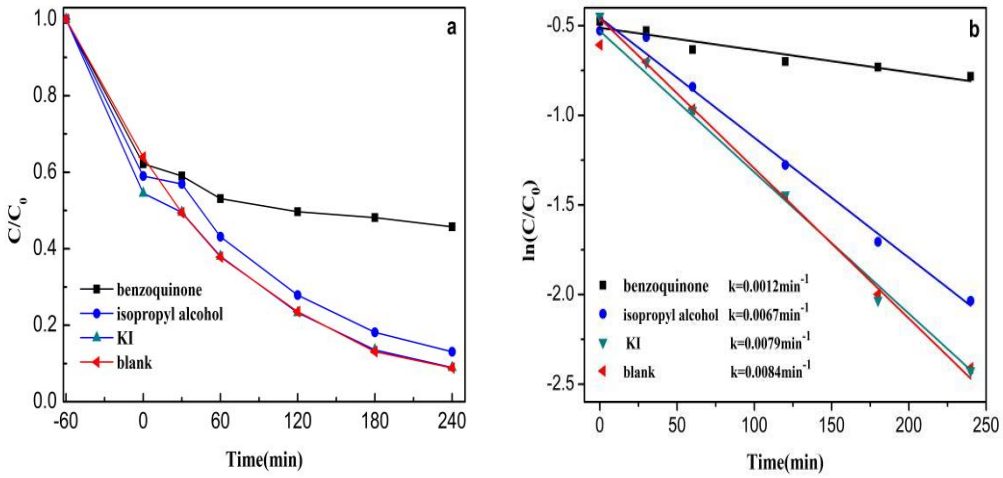

Fig.14. (a) Reactive species trapping experiments of 59% TMCr for BPA degradation, (b) The corresponding removal rate

3.6. Exploration of the intermediate products

In this study, HPLC and HPLC-MS analyses were employed to detect the main intermediates and to propose the possible paths for photocatalytic degradation system (Fig. S9 and S10). In order to better detect intermediates, we focused on the time points of six reaction processes (0, 30, 60, 120, 180 and 240 minutes). Three main intermediates were identified by HPLC-MS. During the first 30 min of the reaction, the concentration of BPA (m/z=227) reduced, but the concentration of 4-hydroxybenzaldehyde (m/z=121, product A) increased dramatically, revealing the initial degradation of BPA. Immediately after, the concentration of product A slightly increased and 3-hydroxybisphenol A (m/z=243, product B) appeared. With the continued increase of reaction times, the concentration of BPA and product A clearly decreased and a new intermediate (m/z=426, product C) appeared.

Based on variation of concentration with reaction time based on three aromatic intermediates, the photo-degradation of BPA went through two possible pathways (I-II) and the corresponding pathways were proposed in Fig. 15. At the beginning, the immediate ring cleavage by ·OH attack BPA to form 4-isopropanolphenol. Then, 4-isopropanolphenol are followed cleavage to form hydroquinone and 4-hydroxybenzaldehyde (product A) [42,43]. Finally, 4-hydroxybenzaldehyde

as the main intermediate was mineralized into CO_2 and H_2O under the action of $\cdot O_2^-$. Moreover, ·OH attacks BPA to form another intermediate 3-hydroxybisphenol A (product B), which has been verified by predecessors [43,44]. Subsequently, product B reacts with hydroquinone to form product C.

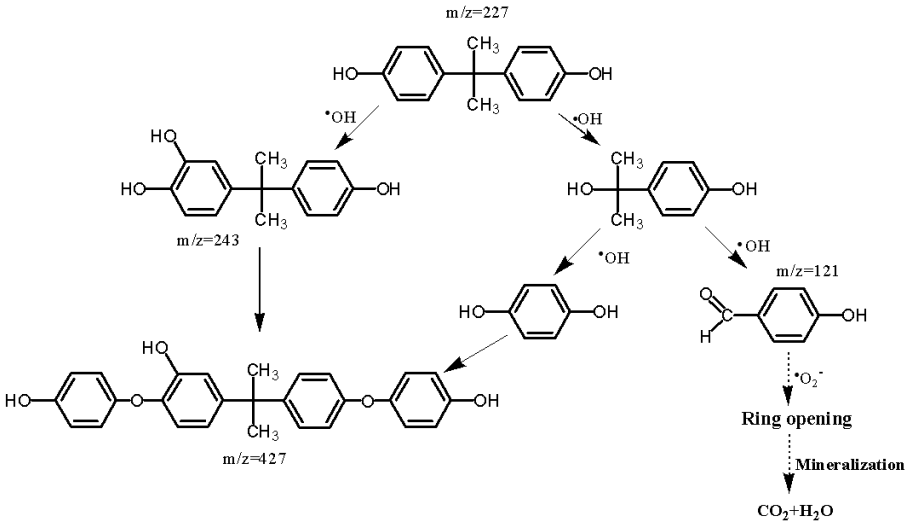

Fig.15. The corresponding degradation pathways of BPA by TMCr

3.7. Photocatalytic degradation mechanism

The remarkably improved photocatalytic degradation activity of the composite than that of physically mixed TiO_2+Cr-MIL was attributed to the synergy between TiO_2 and Cr-MIL. To explore the conduction and valence positions of TiO_2 and Cr-MIL, the band position (E_{CB}) was explored by Mott-Schottky (M-S) measurements. The positive slope observed from the M-S curve reveals the n-type semiconductor properties of TiO_2 (Fig. 16). The E_{CB} of TiO_2 is ~-0.69 V vs Ag/AgCl (-0.49 V vs NHE). With the band gap (Eg) value of TiO_2 estimated to be 3.2 eV from Tauc plot (Fig. 6b), the conduction band position (E_{VB}) was calculated to be 2.76 V vs NHE. Moreover, the E_{CB} of Cr-MIL is ~-0.92V vs Ag/AgCl (-0.72 V vs NHE). With the band gap (Eg) value of TiO_2 estimated to be 2.8 eV, E_{VB} of Cr-MIL was calculated to be 2.08 V vs NHE.

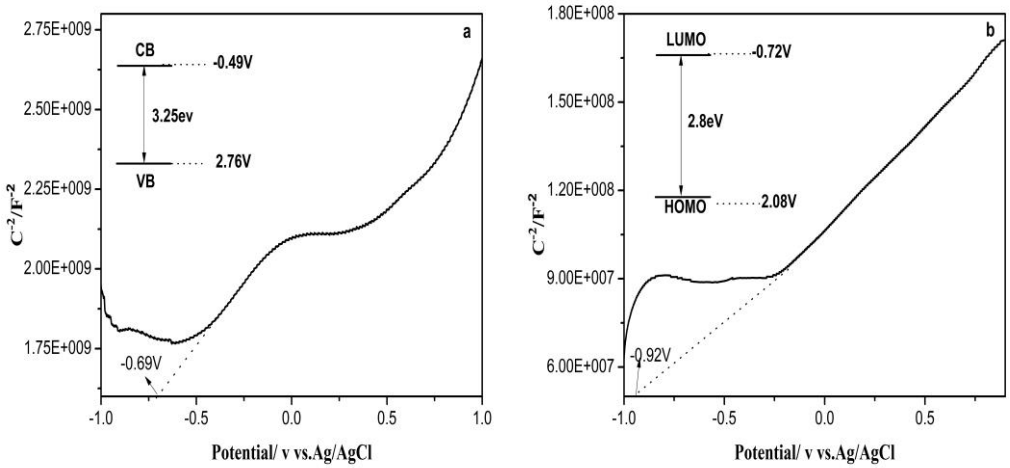

Fig.16. M-S curve of (a) TiO_2 and (b) Cr-MIL

As shown in Fig. 17, the photocatalytic degradation mechanism for degradation of BPA by 59% TMCr was proposed. Firstly, light stimulates Cr-MIL and TiO_2 to generate electrons and holes, respectively. Immediately after, photogenerated electrons are transferred from the conduction band (CB) of Cr-MIL to TiO_2, and photogenerated holes are transferred from the valence band (VB) of TiO_2 to Cr-MIL through the interaction between Cr-MIL and TiO_2. The charge transfer occurs between TiO_2 and Cr-MIL, thus inhibits the electron-hole recombination and enhances the photocatalytic degradation efficiency. The conduction band position of TiO_2 is more negative than the $\cdot O_2^-$ potential ($\cdot O_2^-/O_2$= -0.33V vs NHE), so the photogenerated electrons stored on the CB of TiO_2 can react with the water-dissolved O_2 to generate $\cdot O_2^-$, thereby degrading BPA [45]. Furthermore, portion of -OH react to form ·OH radicals, which is the main reason for hydroxylation and cracking of BPA. These radicals attack the BPA and produce some intermediates. Finally, the intermediates can be further mineralized into CO_2 and H_2O.

$$MIL\text{-}101(Cr)+hv \longrightarrow h^+(MIL\text{-}101(Cr))+e^-(MIL\text{-}101(Cr))$$

$$TiO_2+hv \longrightarrow h^+(TiO_2)+e^-(TiO_2)$$

$$h^+(MIL\text{-}101(Cr))+OH^- \longrightarrow \cdot OH$$

$$e^-(TiO_2)+O_2 \longrightarrow \cdot O_2^-$$

$$\cdot O_2^-/\cdot OH + BPA \longrightarrow CO_2+H_2O$$

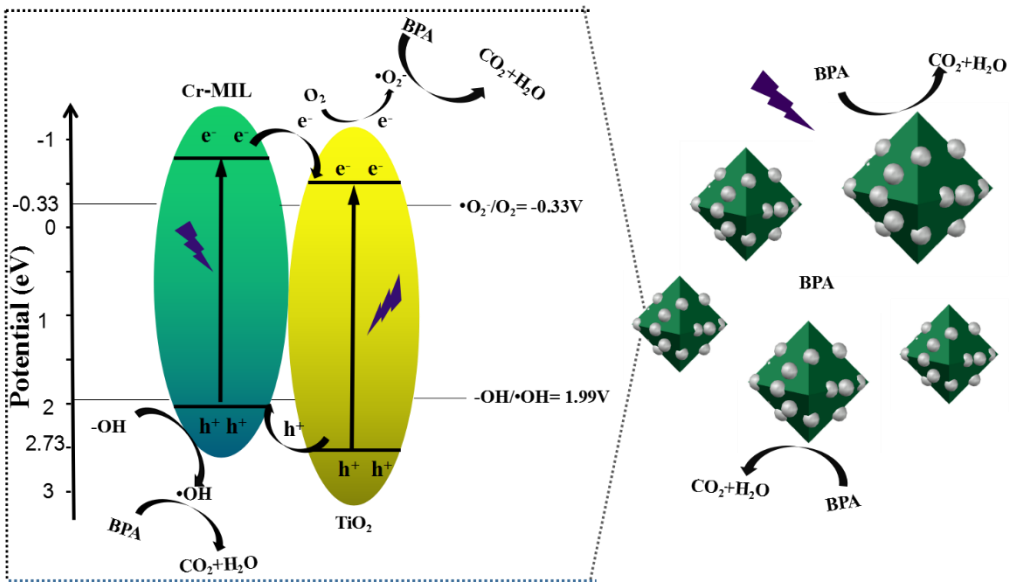

Fig.17. The photocatalytic degradation mechanism for degradation of BPA

4. Conclusion

A series of novel anatase TMCr nanocomposite was synthesized by a facile solvothermal method and were employed in the photocatalytic degradation of BPA. The as-prepared catalysts were characterized by XRD, SEM, BET, EDS, UV-Vis, TEM, XPS, PL analysis and Mott-Schottky to indicate the chemical structure and combination between anatase TiO_2 and Cr-MIL. The introduction of TiO_2 into Cr-MIL not only facilitates the separation of charge carriers at the interface, but also adjusts the surface area of the composites. 59% TMCr had superior photocatalytic degradation performance, and 90% BPA degradation and 80% mineralization were achieved after 240 min under UV irradiation. The TiO_2 content, initial pH value, catalyst dosage and initial BPA concentration all had a real influence on the degradation of BPA. Under optimized conditions, 59% TMCr could reach 99.4% BPA degradation and the corresponding rate constant (k) was 0.0138 min^{-1}. This composite exhibited the excellent stability and recyclability. The three intermediates were detected by HPLC-MS and the BPA photocatalytic degradation pathways was proposed. The oxidative radicals experiment verified $•O_2^-$ plays a dominant role in this system and the photocatalytic degradation mechanism was also proposed.

Acknowledgement

We genuinely appreciate financial support by the National Natural Science Foundation of China (NSFC, No. 21176192 and 21776220), the Tianjin Natural Science Foundation (No.19JCZDJC37600) and Training Project of Innovation Team of Colleges and Universities in Tianjin (TD13-5020).

References

[1] Kasprzykhordern, B; Dinsdale, R M; Guwy, A J. Water Research. 2009, 43, 363-380. doi: 10.1016/j.watres.2008.10.047

[2] Markman, S; Guschina, I. A; Barnsley, S. Chemosphere, 2008, 70, 119-125. doi: 10.1016/j.chemosphere.2007.06.04

[3] Dehghani, M. H; Mahvi, A. H; Rastkari, N. Water. Treat. 2015, 54, 84-92. doi:10.1080/19443994.2013.876671

[4] Guo, W; Wei, H. U; Pan, J. Chem. Eng. J. 2011, 171, 603-611. doi: 10.1016/j.cej.2011.04.036

[5] Choi, Y. J; Lee, L. S. Environ. Sci. Technol. 2017, 23, 13698-13704. doi: 10.1021/acs.est.7b03889.

[6] Eio, E. J; Kawai, M; Tsuchiya, K. Biodeter. Biodegr. 2014, 96, 166-173. doi: 10.1016/j.ibiod.2014.09.011

[7] Fei, L; Qian, L; Zhang, Y. Chem. Eng. J. 2015, 262, 989-998. doi: 10.1016/j.cej.2014.10.046

[8] Guo, C; Ge, M; Liu, L. Environ. Sci. Technol. 2010, 44, 419-25. doi: 10.1021/es9019854

[9] Chen, F; Zhao, J; An, W. RSC Adv. 2017, 7, 39814-39823. doi: 10.1039/c7ra06126a

[10] Chen, F; An, W; Li, Y. Appl. Surf. Sci. 2018, 427, 123-132. doi: 10.1016/j.apsusc.2017.08.146

[11] Kondrakov, O; Ignatev, N; Frimmel, H. Appl. Catal. B. Environ. 2014, 160-161, 106-114. doi: 10.1016/j.apcatb.2014.05.007

[12] Doong, A; Liao, C. J. Hazard. Mater. 2017, 322, 254-262. doi: 10.1016/j.jhazmat.2016.02.065

[13] Mu, C; Yu, Z; Cui, W. Appl. Catal. B. Environ. 2017, 212, 41-49. doi: 10.1016/j.apcatb.2017.04.018

[14] Cao, F; Xiong, J; Wu, F. Appl. Mater. Inter. 2016, 8, 12239. doi:10.1021/acsami.6b03842

[15] Yoshihisa, O; Isao, A; Chisa, N. Environ. Sci. Technol, 2001, 35, 2365-8. doi:10.1021/es001757t

[16] Yuan, Z; Jia, J; Zhang, L. Mater. Chem. Phys. 2002, 73, 323-326. doi:10.1016/S0254-0584(01)00373-X

[17] Low, W; Boonamnuayvitaya, V. J. Environ. Manage. 2013, 127, 142-149. doi:

10.1016/j.jenvman.2013.04.029

[18] Kolobov, S; Svintsitskiy, A; Kozlova, A. Chem. Eng. J. 2017, 314, 600-611. doi: 10.1016/j.cej.2016.12.018

[19] Guo, H; Kemell, M; Heikkilä, M. Appl. Catal. B. Environ. 2010, 95, 358-364. doi: 10.1016/j.apcatb.2010.01.014

[20] Wang, Y; Zhong, M; Chen, F. Appl. Catal. B. Environ. 2009, 90, 249-254. doi: 10.1016/j.apcatb.2009.03.032

[21] Crake, A; Christoforidis, C; Kafizas, A. Appl. Catal. B. Environ. 2017, 210, 131-140. doi: 10.1016/j.apcatb.2017.03.039

[22] Spanopoulos, I; Tsangarakis, C; Klontzas, E; Tylianakis, E; Froudakis, G; Adil, K. J. Am. Chem. Soc. 2015, 138, 12239 – 12245. doi:10.1021/jacs.5b11079

[23] Yuan, P, Yin, S; Cao, W. Appl. Catal. B. Environ. 2015, 168-169, 572-576. doi: 10.1016/j.apcatb.2014.11.007

[24] Hod, I; Sampson, M. D; Deria, P; Kubiak, C. P; Farha, O. K; Hupp, J. T. ACS Catal. 2015, 5, 6302 – 6309. doi:10.1021/acscatal.5b01767

[25] Hong, Y; Hwang, K; Serre, C. Adv. Funct. Mater. 2009, 19, 1537-1552. doi:10.1002/adfm.200801130

[26] Wen, M; Mori, K; Kamegawa, T. Chem. Commun. 2014, 50, 11645-11648. doi:10.1039/c4cc02994a

[27] Chang, N; Zhang, H; Shi, M. S; Li, J. Mater. Lett. 2017, 200, 55-58. doi: 10.1016/j.matlet.2017.04.099

[28] He, J; Yan, Z; Wang, J. Chem. Commun. 2013,49, 6761-6763. doi:10.1039/c3cc43218a

[29] Xu, Y; Qi, C; Yang, H. Mat. Sci. Semicon. Proc. 2015, 36, 115-123. doi: 10.1016/j.mssp.2015.03.025

[30] Jiang, Z; Liu, J; Gao, M. Adv. Mater. 2017, 29, 1603369. doi:10.1002/adma.201603369

[31] Li, X; Pi, Y; Xia, Q. Appl. Catal. B. Environ. 2016, 191, 192-201. doi: 10.1016/j.apcatb.2016.03.034

[32] Sheng, H; Chen, D; Li, N. Chem. Mater. 2017, 29, 5612-5616. doi: 10.1021/acs.chemmater.7b01243

[33] Gong, Y; Yang, B; Zhang, H. J. Mater. Chem. A. 2018, 46, 23703-23711. doi:

10.1039/c8ta07915c

[34] Zhang, Y; Chen, Z; Zhou, L. Environ. Pollut. 2019, 244, 93-101. doi: 10.1016/j.envpol.2018.10.028

[35] Ferey, G. A, Science. 2005, 309, 2040-2042. doi: 10.1126/science.1116275

[36] Lee, Y; Kim, S; Kang, J. K. Chem. Commun. 2015, 51, 5735-5738. doi: 10.1039/C5CC00686D

[37] Sun, Z; Liao, T; Dou, Y; Hwang, S. M; Park, M. S; Jiang, L; Kim, J. H; Dou, S. X. Nat. Commun. 2014, 5, 3813-3841. doi: 10.1038/ncomms4813

[38] Zhang, N; Zhang, Y; Pan, X. J. Phys. Chem. C. 2012, 116, 18023-1803. doi:10.1021/jp303503c

[39] Wang, J. J; Yang, M; Dong. W. J. Catal. Sci. Technol., 2016, 6, 161-168. doi: 10.1039/C5CY01099C

[40] Chen, F; An, W; Li, Y. Appl. Surf. Sci. 2018, 427, 123-132. doi: 10.1016/j.apsusc.2017.08.146

[41] He, J; Yan, Z; Wang, J; Xie, J. Jiang, L; Shi, Y; Yuan, F; Yu, F; Sun. Y. Chem. Commun., 2013, 49, 6761-6763. doi:10.1039/C3CC43218A

[42] Liu, Y; Mao, Y; Tang, X. Chinese J. Catal. 2017, 38, 1726-1735. doi:10.1016/S1872-2067(17)62902-4

[43] Shi, H; Shi, S; Ra, M. Appl. Catal. B. Environ. 2008, 84, 797-802. doi: 10.1016/j.apcatb.2008.06.023

[44] Inoue, M; Masuda, Y; Okada, F. Water Res. 2008, 42, 0-1386. doi: 10.1016/j.watres.2007.10.006

[45] Imai, S; Gamo, S. K. J. Biosci. Bioeng. 2007, 103, 420-426. doi:10.1263/jbb.103.420